

RESEARCH ARTICLE

Open Access



Integrative single-cell RNA-seq analysis of vascularized cerebral organoids

Yuya Sato¹, Toru Asahi^{1,2,3*} and Kosuke Kataoka^{2*}

Abstract

Background Cerebral organoids are three-dimensional in vitro cultured brains that mimic the function and structure of the human brain. One of the major challenges for cerebral organoids is the lack of functional vasculature. Without perfusable vessels, oxygen and nutrient supplies may be insufficient for long-term culture, hindering the investigation of the neurovascular interactions. Recently, several strategies for the vascularization of human cerebral organoids have been reported. However, the generalizable trends and variability among different strategies are unclear due to the lack of a comprehensive characterization and comparison of these vascularization strategies. In this study, we aimed to explore the effect of different vascularization strategies on the nervous system and vasculature in human cerebral organoids.

Results We integrated single-cell RNA sequencing data of multiple vascularized and vascular organoids and fetal brains from publicly available datasets and assessed the protocol-dependent and culture-day-dependent effects on the cell composition and transcriptomic profiles in neuronal and vascular cells. We revealed the similarities and uniqueness of multiple vascularization strategies and demonstrated the transcriptomic effects of vascular induction on neuronal and mesodermal-like cell populations. Moreover, our data suggested that the interaction between neurons and mesodermal-like cell populations is important for the cerebrovascular-specific profile of endothelial-like cells.

Conclusions This study highlights the current challenges to vascularization strategies in human cerebral organoids and offers a benchmark for the future fabrication of vascularized organoids.

Keywords Cerebral organoids, Vascularization, Single-cell RNA sequencing, Meta-analysis

Backgrounds

Pluripotent stem cell-derived human cerebral organoids are self-organized, three-dimensional in vitro cell cultures that mimic the neurodevelopmental processes,

organization, and neural activity of the human cerebral cortex. Advancing methods for generating cerebral organoids have provided unprecedented opportunities for understanding neural development, evolution, and disease [1]. Moreover, in the recent coronavirus disease 2019 pandemic, human organoid models have shown promising outcomes in understanding the pathogenesis of the disease, which potentially served as a key to the development of therapeutic agents against severe acute respiratory syndrome coronavirus 2 infections [2, 3]. Despite the rapid growth in this field, the development of cerebral organoids is still in its infancy, with several limitations hindering its broader applications and greater impact. One of the major challenges is that cerebral organoids

*Correspondence:

Toru Asahi

tasahi@waseda.jp

Kosuke Kataoka

kataokak@aoni.waseda.jp

¹ Graduate School of Advanced Science and Engineering, Waseda University, Tokyo, Japan

² Comprehensive Research Organization, Waseda University, Tokyo, Japan

³ Research Organization for Nano & Life Innovation, Waseda University, Tokyo, Japan



© The Author(s) 2023. **Open Access** This article is licensed under a Creative Commons Attribution 4.0 International License, which permits use, sharing, adaptation, distribution and reproduction in any medium or format, as long as you give appropriate credit to the original author(s) and the source, provide a link to the Creative Commons licence, and indicate if changes were made. The images or other third party material in this article are included in the article's Creative Commons licence, unless indicated otherwise in a credit line to the material. If material is not included in the article's Creative Commons licence and your intended use is not permitted by statutory regulation or exceeds the permitted use, you will need to obtain permission directly from the copyright holder. To view a copy of this licence, visit <http://creativecommons.org/licenses/by/4.0/>. The Creative Commons Public Domain Dedication waiver (<http://creativecommons.org/publicdomain/zero/1.0/>) applies to the data made available in this article, unless otherwise stated in a credit line to the data.

lack vascular systems [4, 5]. In the absence of a perfusable vascular network, cerebral organoids rely solely on passive diffusion to exchange nutrients, oxygen, and toxic metabolites. The lack of vascular systems also limits the size of organoids and triggers apoptotic and/or necrotic cell death in the core of organoids [1]. Furthermore, the differentiation of neural progenitor cells is prevented in organoids lacking vasculature [6].

The cerebral vasculature is an uninterrupted arbor-like network of blood vessels comprising diverse cell types, including endothelial cells (ECs), pericytes, and vascular smooth muscle cells [7]. These cells coordinate to support brain homeostasis in a variety of ways: providing oxygen, energy metabolites, and other nutrients to the brain; removing by-products of brain metabolism; preventing the entry of circulating toxins; and modulating immune responses [8, 9]. During the development of the nervous system, the vascular system contributes to the proper formation and function of the central nervous system and vice versa [10]. Furthermore, the vascular system controls the proliferation and differentiation of neural progenitor cells through the supply of oxygen and nutrients and also serves as a scaffold for the migration of neuroblasts and newborn neurons [11, 12]. Recent studies have proposed that oligodendrocyte precursor cells (OPCs) require blood vessels as scaffolds for migration and that the interaction between OPCs and ECs supports OPC maturation [13].

Multiple strategies have been proposed for the development of vascular systems in human cerebral organoids. In 2018, two groups independently developed robust vascularization of organoid grafts by *in vivo* transplantation of cerebral organoids into mouse brains. Mansour et al. reported the first vascularization strategy of grafting and maintaining cerebral organoids into immune-deficient adult mouse brains for a long term (180 days), in which the organoids exhibited neuronal differentiation and maturation, gliogenesis, microglial integration, and axonal growth into multiple regions of the host brain [14]. The other group (Daviaud et al.) transplanted cerebral organoids into young mice (post-natal day 8–10) without immunosuppressive agents and observed extensive angiogenesis from the host brain into organoid grafts [15].

Furthermore, several protocols have been developed to generate *in vitro* functional vasculatures in human cerebral organoids, which can be broadly classified into three categories (Fig. 1A): (1) co-differentiation with mesodermal progenitors, (2) co-culture with ECs, and (3) assembly of distinct organoids/spheroids. The co-differentiation protocols involve the development of embryonic vasculature, starting with the differentiation of mesoderm-derived angioblasts. This strategy closely

mimics the development of nascent vasculature during organogenesis [16]. In this strategy, mesoderm development can be induced along with the ectoderm to produce vascularized cerebral organoids using a proper combination of growth factors or gene engineering. Ham et al. guided vasculogenesis by supplementing organoids with vascular endothelial growth factor and Wnt7a [17]. On the contrary, Cakir et al. induced vascular systems by overexpressing human ETS variant transcription factor 2 (*hETV2*) in some populations of stem cells. In this protocol, pericyte-like cells were observed in vascularized organoids in addition to ECs [16]. *ETV2* has been extensively studied and utilized to specify cells to endothelial and hematopoietic lineages after the discovery of its capability to convert human skin fibroblasts into functional ECs [18–20].

In co-culture protocols, vascularization is achieved by mixing ECs that have already differentiated during organoid formation. There are two main sources of ECs: human umbilical vein endothelial cells (HUVECs) [21] and induced pluripotent stem cell (iPSCs)-derived ECs [21, 22]). HUVECs, which originate from the human umbilical vein endothelium, are commonly utilized to vascularize organoids, partly because of the ease with which they are obtained and cultured and were exemplified for the first time by the vascularization in liver buds [23]. Shi et al. used HUVECs to obtain vascularized organoids (termed “vOrganoid” in their study) and successfully cultured them for more than 200 days [21].

The assembly of distinct organoids/spheroids, or assembloids, involves docking cerebral organoids with vascular organoids/spheroids, which are separately differentiated from human embryonic stem cells or iPSCs [24, 25]. Unlike other vascularized cerebral organoids, the assembloid proposed by Sun et al. achieved simultaneous immunization and vascularization [24]. Because blood vessels exhibit large heterogeneity of functions among tissues [26], Sun et al. induced specific cerebrovascular features in their vascular organoids by adding neurotrophic factors during the maturation step of vascular organoids, followed by the fusion of brain and vascular organoids [24].

The studies described above proposed different strategies for inducing vascularization in human cerebral organoids, in which the functions, structures, cellular compositions, and cell–cell interactions in the organoids have been independently analyzed. However, no studies have synthetically compared the impacts of these vascularization methods on the diverse cells that comprise vascularized cerebral organoids. Here, we evaluated multiple vascularized human cerebral organoids generated by different strategies through an integrated comparison of single-cell RNA sequencing (scRNA-seq) data available

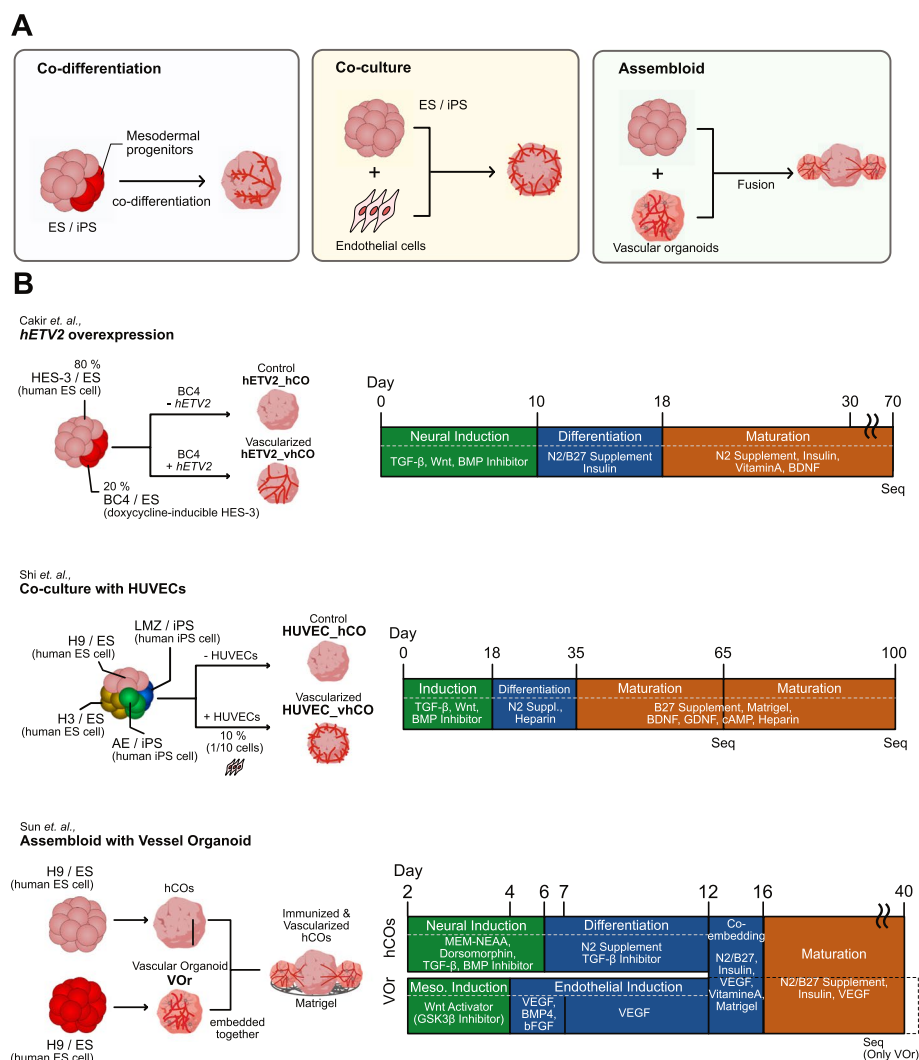


Fig. 1 Comparison of vascularization strategies. **A** Three vascularization strategies. Left panel: co-differentiation (differentiation with mesodermal cells), middle panel: co-culture (co-culture with endothelial cells), right panel: assembloid (fusion with vascular organoids). **B** Detailed protocols of the vascularization methods we focused on in this study

in public datasets and fetal brains. The present study provides insights into the effects of multiple vascularization strategies on cell type differentiation and transcriptomic profiles in neuronal and vascular cells. The findings of this study will provide a benchmark for the fabrication of vascularized cerebral organoids in the future.

Results

Dataset description

We collected publicly available scRNA-seq datasets of human cerebral organoids, which comprised the following three samples: (1) *hETV2* knock-in vascularized organoids [16], (2) HUVEC co-cultured organoids [21], and (3) vascular organoids (VOr) used for the assembloid

[24] (Table 1, Fig. 1A). The first two samples ((1) and (2)) included non-vascularized organoids as controls [16, 21]. As described in the “Backgrounds” section, the vascularization strategies reported in these three studies [16, 21, 24] were based on three major categories of engineering organoids with functional vasculature (i.e., co-differentiation with mesodermal progenitors, co-culture with ECs, and assembly of distinct organoids/spheroids, respectively) (Fig. 1A). The scRNA-seq data from the studies by Cakir et al. and Shi et al. were derived from cerebral organoids that contained induced vasculatures, whereas the data from Sun et al. were derived only from vascular organoids with induced cerebrovascular features for further fusion with cerebral organoids. An overview of

Table 1 Summary of datasets used in this study

Protocols	Authors	Phenotype	SRA Accession ID/GEO Datasets ID	Day
<i>hETV2</i> overexpression	Cakir et al	Non-vascularized cerebral organoid Vascularized cerebral organoid	SRS5079104 SRS5079105	70 days
Co-culture with HUVEC (65 d)	Shi et al	Non-vascularized cerebral organoid Vascularized cerebral organoid	SRS6066824; SRS6066825; SRS4752357 SRS6066826; SRS6066827; SRS4752359	65 days
Co-culture with HUVEC (100 d)	Shi et al	Non-vascularized cerebral organoid Vascularized cerebral organoid	SRS4752358; SRS6066828; SRS6066829 SRS4752360; SRS6066830; SRS6066831	100 days
Assembloid (Fetal brain)	Sun et al Trevino et al	Vascular organoid (Fetal brain)	SRR15992285; SRR15992286 GSM4944143; GSM4944144 GSM4944145; GSM4944146 GSM4944147; GSM4944148 GSM4944149; GSM4944150	40 days PCW16 PCW20 PCW21 PCW24

SRA Accession ID; identifier of the NCBI Sequence Read Archive database

GEO Datasets ID; identifier of the NCBI Gene Expression Omnibus database

the protocols by which these organoids were produced is shown in Fig. 1B. We also included scRNA-seq datasets from the human fetal cerebral cortex on 16, 20, 21, and 24 post-conceptual weeks (PCW) [27]. We used a combined dataset from all the different PCWs for further analysis.

For pre-processing, we first filtered out low-quality cells from the scRNA-seq datasets (Additional file 1: Fig. S1A and S1B). We then independently analyzed each sample by projecting the cells in each sample into an adjusted 2D space using Uniform Manifold Approximation and Projection (UMAP) and then labeling with any of the 12 cell types based on cell-type-specific marker gene expression, including *SOX2*⁺ progenitor cell (PROG), *TOP2A*⁺/*BIRC5*⁺ proliferating cell (PC), *EOMES*⁺ intermediate progenitor cell (IPC), *TUBB3*⁺/*RBFOX3*⁺ unspecified neuron (Neuron), *GAD1*⁺/*GAD2*⁺ inhibitory neuron (IN), *SLC17A6*⁺/*SLC17A7*⁺ excitatory neuron (EX), *GFAP*⁺/*AQP4*⁺ astrocyte (AS), *OLIG1*⁺/*OLIG2*⁺ oligodendrocyte progenitor cells (OPC), *RBFOX3*⁻/*COL1A1*⁺, *ACTA2*⁺, *RGS5*⁺, *CLDN5*⁺ vascular-related-like cell (VLC), *CD53*⁺/*CX3CR1*⁺ microglia-like cell (MGLC), *DDIT3*⁺ unfolded protein response cells (UPRC), and unknown cells (Unknown) (Fig. 2A, B and Additional file 2: Fig. S2A–S2H). A total of 147,978 cells from multiple samples were integrated based on the feature genes and then visualized using UMAP (Fig. 2A and Additional file 3: Fig. S3A–S3D).

Cell type compositions in vascularized, non-vascularized, and vascular organoids

The annotation strategy of the 12 cell types is shown in Additional file 4: Fig. S4A. Each assigned cell type specifically expressed the marker genes (Fig. 2B). Moreover, the top 100 genes enriched in each cell type scarcely overlapped, suggesting that the assigned cell types were

independent populations, representing separate transcriptomic profiles (Additional file 4: Fig. S4B). Additionally, genes specifically expressed in PROGs, neuronal cell types (IPC, Neuron, IN, and EX), and VLCs were shared with those expressed in the fetal brain, suggesting that the characteristics of each cell type in the organoids were similar to those of the fetal brain at the transcriptomic level (Additional file 5: Fig. S5A).

Next, we sought to identify differences in cell composition with vascularization by calculating the percentage of cell type occupancy in each sample. Except for that in VOr, a relatively large occupancy of the following cell types was observed PROG, PC, IN, and EX in all organoids (Fig. 2B, C). Notably, we found that major changes in cell composition were induced by the protocols or days of culture rather than by vascularization (Fig. 2C and Additional file 5: Fig. S5B). For instance, the organoids in Cakir et al.'s study were characterized by a high ratio of VLC and the presence of AS [16]. In contrast, those in Shi et al.'s study at day 65 of culture were characterized by a low ratio of VLC and the absence of AS, while a prolonged culture period induced AS and OPC in the organoids [21], which might be due to the increased diversity of cell types with the time of growth [28] (Fig. 2B, C). These findings suggest that major cell types in the organoids are minimally impacted by vascularization.

Cell populations with non-microglial mesoderm-like expression were assigned to VLCs, which cannot be classified into any cell type in ectodermal lineages such as neurons and astrocytes. Most of the cells in the VOr were classified as VLC with the expression of *CLDN5*, *COL1A1*, *RGS5*, and *ACTA2* (Fig. 2B, C, and Additional file 4: Fig. S4H), as VOr solely comprised the vascular system. We also identified VLCs in organoids from Cakir and Sun's studies (Fig. 2B, C). The lack of dual-SMAD

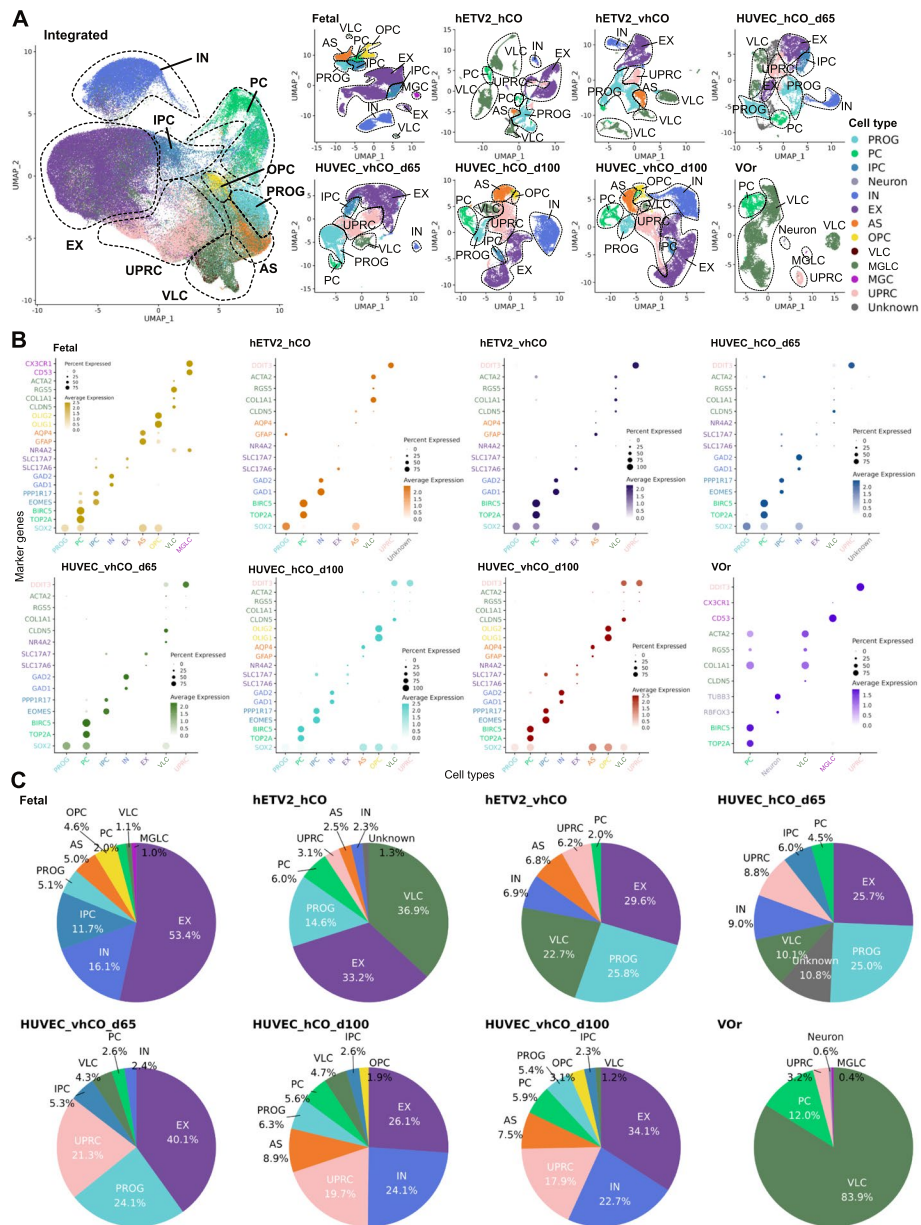


Fig. 2 Mapping of scRNA-seq data from non-vascularized organoids and fetal brain to UMAP with cell types. **A** UMAP visualization of transcriptomes with cell types. Left panel: UMAP integrated scRNA-seq data for all samples, right panel: UMAP for each sample. Assigned cell types are as follows: PROG; Progenitors (*SOX2*⁺), PC; Proliferating Cells (*TOP2A*⁺, *BIRC5*⁺), IPC; Intermediate Progenitor Cells (*EOMES*⁺, *PPP1R17*⁺), Neuron (*RBFOX3*⁺, *TUBB3*⁺), IN; Inhibitory Neurons (*GAD1*⁺, *GAD2*⁺), EX; Excitatory Neurons (*SLC17A6*⁺, *SLC17A7*⁺), AS; Astrocytes (*GFAP*⁺, *AQP4*⁺), OPC; Oligodendrocyte Progenitor Cells (*OLIG1*⁺, *OLIG2*⁺), VLC; Vascular-Related-Like Cells (*CLDN5*⁺, *COL1A1*⁺, *RGSS5*⁺, *ACTA2*⁺), MGLC; Microglia-like Cells (*CD53*⁺, *CX3CR1*⁺), and UPRC; Unfolded Protein Response Cells (*DDIT3*⁺). **B** Expression of marker genes of each cell type in each sample. The cell type is displayed on the x-axis, and the marker gene for each cell type is displayed on the y-axis. The color of the marker corresponds to the color of each cell type. hCO; human cerebral organoids, and vhCO; vascularized hCO. **C** Ratio of cells present in each sample. The ratio is calculated as the percentage of each cell count to the total cells in each sample

inhibition (inhibition of BMP and TGF- β) during the generation of cerebral organoids can lead to the formation of mesoderm-derived progenitors [29, 30]. Nevertheless, Cakir and Sun’s studies applied LDN-193189 and SB-431542 to inhibit BMP/TGF- β signaling in neural

induction processes, suggesting that cerebral organoids innately develop VLCs irrespective of dual-SMAD inhibition or vasculature induction. Another challenge for human cerebral organoids is the absence of microglia and vascularization [31]. MGLC

were absent from cerebral organoids in Cakir et al.'s [16] and Shi et al.'s [21] studies, whereas they were found in VOr in the study by Sun et al. [24] (Fig. 2C). However, MGLC in VOr expressed only partially the microglia-specific markers. There were some markers (*MERTK*, *TGFBR1*, *GPR34*, and *HEXB*) expressed, for example, but not others (*TYRO3*, *PROS1*, *OLEML3*, *TMEM119*, and *SALL1*) (Additional file 5: Fig. S5C). This result suggests that immunization is achievable but only partial by the vascularization of cerebral organoids, according to the protocol of Sun's study. In addition, VOr contained a small number of *RBFOX3*⁺/*TUBB3*⁺ neuronal cell clusters (Fig. 2B, C). This cluster lacked the typical EX and IN marker genes. These neurons that developed in the VOr may be, therefore, off-target immature neurons that have differentiated by the supplement of N2/B27 from undifferentiated cells during the maturation process.

Overall, we identified the diversity of cell types in vascularized organoids, including newly discovered mesodermal cells, and protocol- or culture-time-dependent heterogeneity of cell types.

Diverse vascularization protocols trigger different transcriptomic alterations in human cerebral organoids

We next examined whether different vascularization strategies influence the fidelity of organoids to the human fetal brain. To this end, we calculated the correlations of "enrichment score" in each cell type in organoids and the human fetal brain (see "Methods"). All vascularization protocols improved the correlations in most cell types, suggesting that vascularization generally advances organoid fidelity to the human fetal brain (Fig. 3A). Nevertheless, the transcriptomic similarities of VLCs in the VOr were not as high (0.22; Fig. 3A) as those of the organoids in previous studies [16, 21], suggesting that treatment with neurotrophic factors to induce cerebrovascular features in the VOr was insufficient to reproduce brain-specific VLC.

Next, we investigated the bulk transcriptomic alterations triggered by different vascularization methods. The calculation of the number of genes whose expression levels were significantly altered by vascularization identified 4260 upregulated and 2449 downregulated genes. Overexpression of *hETV2* upregulated 3305 genes, whereas co-culture with HUVECs upregulated only 1306 genes at 60 days and 465 genes at 100 days (Fig. 3B). These differences suggested that *hETV2* activates diverse biological processes. The number of genes commonly upregulated and downregulated in the three samples was 38 and 24, respectively (Fig. 3B and Additional file 6: Table S1). The commonly upregulated genes were related to neuronal development and axonogenesis, including *TMEM35A*, *EEF1A2*, and

BASPI [32–34]. The commonly downregulated genes were related to neurotoxicity, such as *MT-ATP6*, *SERPINH1*, and *IGFBP5* [35–37]. These results imply that vascularization increases neural activity and suppresses cellular stress, although a few processes are consistently altered across protocols.

We predicted overrepresented biological processes using gene set enrichment analysis (GSEA) based on the significant differentially expressed genes (adjusted *p*-value < 0.01) between non-vascularized and vascularized organoids (Fig. 3C, D, Additional file 7: Fig. S6 and Additional file 8: Table S2). GSEA revealed that overexpression of *hETV2* downregulated collagen-containing extracellular matrix, actin binding, and contractile contraction development, while it upregulated anterior/posterior pattern specification (Fig. 3D). Downregulated genes included extracellular matrix-related genes, such as collagen family genes (*COL1A1*, *COL1A2*, *COL3A1*), fibulin (*FBLN1*), and proteoglycans (*BGN*, *DCN*); actin binding-related genes, including *ACTA2* and *ACTC1* (actin family genes); and muscle function-related genes, including troponin family genes (*TNNT1*, *TNNT2*, *TNNC1*, *TNNC2*), myosin family genes (*MYLIP* and *MYL4*), and transgelin (*TAGLN*). *ETV2* is known to directly reprogram fibroblasts or muscle cells into vascular ECs [18, 38]. The observed downregulation of the extracellular matrix and muscle development by *hETV2* overexpression might be due to its transdifferentiation capability. GSEA also revealed that the anterior/posterior pattern specification process was upregulated, in which the expression of homeobox family genes (*HOXA2*, *HOXB2*, *HOXB5*, *HOXB6*, *HOXB7*, *HOXC6*, *HOXA9*, *HOXA10*, *HOXC10*) was enhanced as previously reported [16]. In contrast, the genes encoding the electron transport chain (*COX5B*, *CYCS*) and ribosomal proteins (*RPL39*, *RPS29*, *RPL36*, *RPL37A*, *RPS27*, *RPL36*, *RPL36A*, *RPS28*, *RPL38*, *RPS27L*, *RPS24*) were upregulated in HUVEC co-cultured with organoids (Fig. 3C, D), which indicated the availability of sufficient nutrient supply by HUVEC vascularization. Moreover, after 100 days of HUVEC culture, the expression of hypoxia markers *BNIP3* and *SLC2A1* (protein: GLUT-1) and an unfolded protein response marker *DDIT3* was significantly downregulated, indicating that HUVEC co-culture suppressed the hypoxic stress. These results suggest that vascularization with HUVECs potentially improves oxygen and nutrient supply, leading to cellular stress suppression, whereas *hETV2* overexpression regulates cell differentiation capacity and regional patterning. Taken together, these studies imply that vascularization increases the fidelity of cell differentiation in cerebral organoid strategy-dependently.

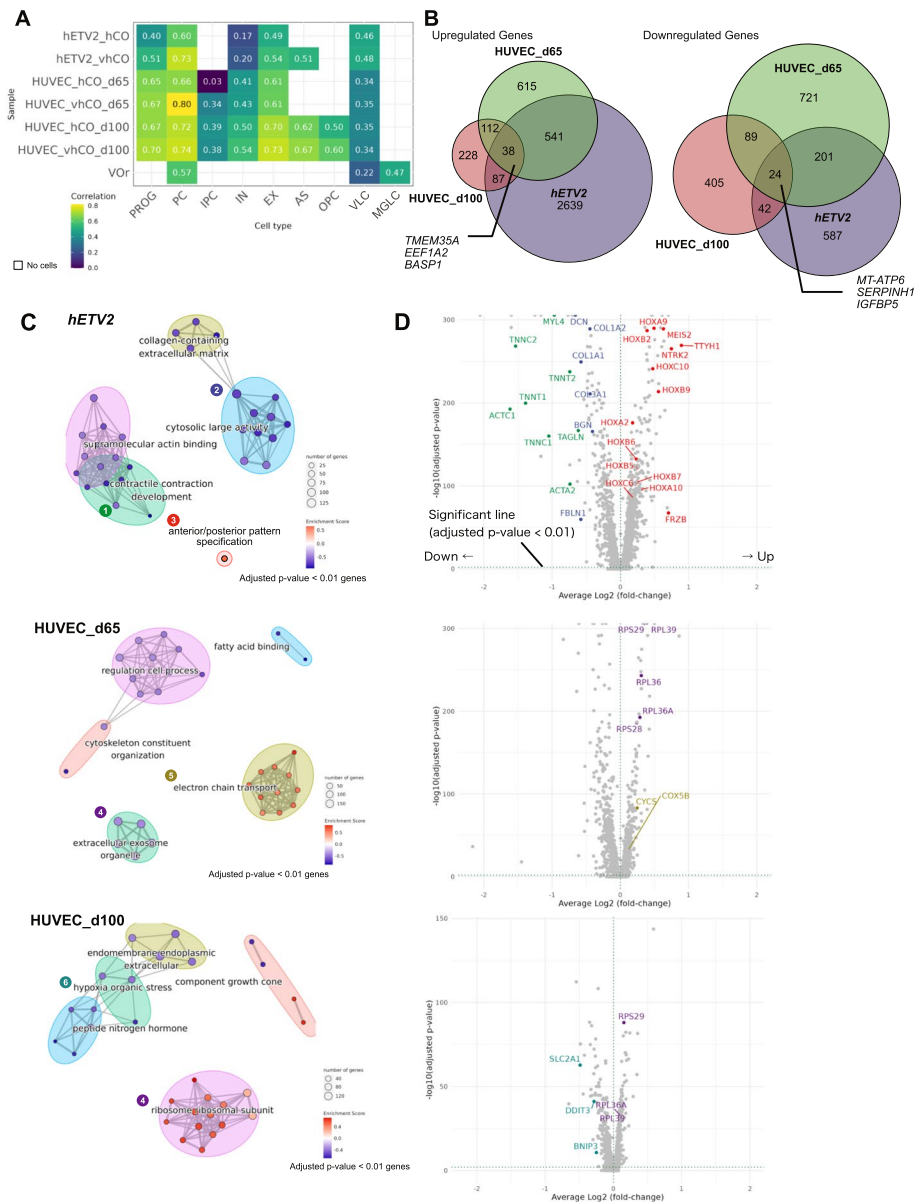


Fig. 3 Transcriptomic fidelities in the fetal brain and bulk alteration transcriptomic by vascularization. **A** Similarity of transcriptome profiles in the fetal brain. Higher correlation values indicate higher similarity. Blank cells indicate the absence of cells [Refer to “Methods” section for the calculation of the correlation values]. **B** Venn diagrams of genes altered by vascularization. Numbers indicate the number of genes changed. Left panel: Venn diagram of upregulated genes, right panel: Venn diagram of downregulated genes. Genes pointing to the center represent examples of genes commonly altered by vascularization in all vascularization protocols. **C** Significantly altered gene ontology (GO) terms (p -value < 0.05) predicted by gene set enrichment analysis (GSEA) of genes significantly altered by vascularization (corrected p -value < 0.01). The color of the nodes represents the enrichment score (the amount of change calculated by GSEA). The edge width between the nodes represents the similarity of gene set pairs. **D** Volcano plot of genes with altered expression induced by vascularization. The average \log_2 fold-change (FC) is shown on the x-axis and the $-\log_{10}$ (corrected p -value) is on the y-axis. The color of the gene names corresponds to the color of the GO terms in **C**

Different vascularization protocols uniquely influence the transcriptome of neuronal populations in cerebral organoids

The cerebral organoids in Cakir’s (*hETV2* overexpression) and Shi’s (HUVEC co-culture) studies produced

three neuronal subtypes: EX, IN, and intermediate progenitor cells (IPC). Therefore, we set out to characterize the effect of these vascularization methods on the transcriptomic profile, with a focus on these neuronal populations. Datasets derived from VOR were excluded

from this analysis because they contained few neuronal cells. First, we extracted and re-clustered neural cells and then projected them into UMAP (Additional file 9: Fig. S7A). The analysis revealed *hETV2* overexpression-mediated vascularization increased the proportion of IN (*GAD1⁺/GAD2⁺*) from 6.6 to 18.9%

(Fig. 4A). In contrast, vascularization achieved by co-culture with HUVECs increased the proportion of EX (*SLC17A7⁺/KCNJ1⁺*) from 66.1 to 83.9% on 65 days and from 49.5 to 57.7% on 100 days (Fig. 4A). These results indicated vascularization methods also alter the proportions of neuronal subtypes.

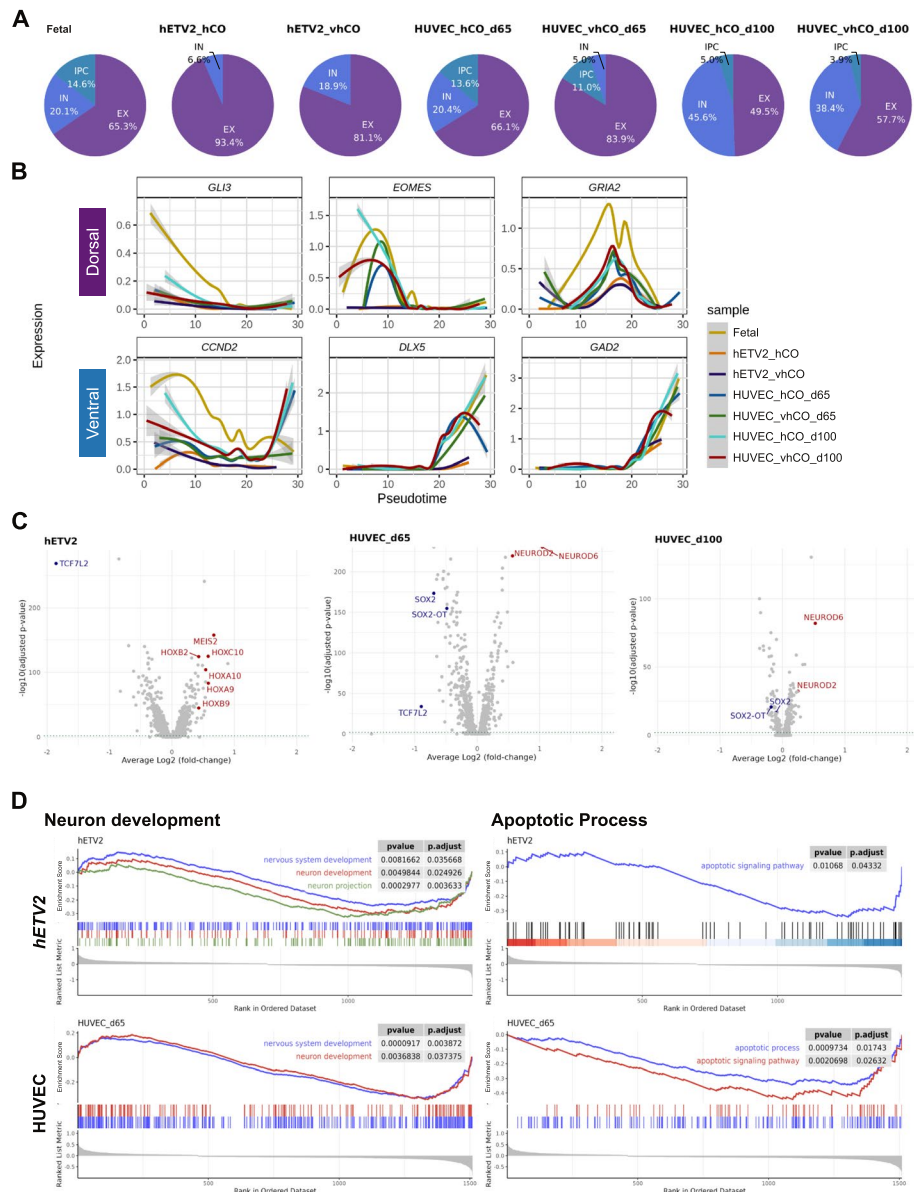


Fig. 4 Protocol-dependent differences in transcriptomic profiles in neuronal cell populations. **A** Percentage of neuronal subtypes in each sample. **B** Changes in expression levels of genes characteristic of dorsoventral development along pseudotime. The pseudotime was calculated with predicted differentiation trajectories of the following cells: PROG, PC, IPC, Neuron, IN, EX, AS, and OPC. The gray shading indicates confidence intervals computed by the generalized additive model approximation. **C** Volcano plot of gene expression altered by vascularization in neurons. **D** GSEA plots of GO terms predicted from the significantly altered (adjusted p -value < 0.01) gene groups. Left panel: GO terms involved in neurodevelopment (nervous system development, neuron development, neuron projection), right panel: GO terms involved in apoptosis (apoptotic signaling pathway). In HUVEC co-culture samples for 100 days, GO terms were not predicted because of the low number of genes altered by vascularization

In the developing fetal brain, cortical EXs are generated locally in the dorsal forebrain, whereas INs are generated in the ventral forebrain and migrate to the cortex [39]. To uncover the underlying molecular mechanisms of the differences in neuronal subtype differentiation, we analyzed the changes in the expression of dorsal- and ventral-specific neurogenic genes over time. To predict the pseudotime, ectodermal cells (IPC, Neuron, EX, IN, AS, and OPC) plus PROG and PC were extracted and re-clustered, followed by the construction of pseudo-differentiation trajectories (Additional file 9: Fig. S7B). Vascularization had insignificant effects on the temporal expression patterns of most neurogenic genes, except for *EOMES* (Fig. 4B). *EOMES* (protein: Tbr2) is specifically expressed in IPCs, which are derived from radial glial progenitors and neural stem cells of the developing cortex, and serve as excitatory neurogenic progenitors [40, 41]. As shown in Fig. 4B, *EOMES* expression was enhanced in a specific developmental time window in the 65-day HUVEC co-cultured organoid [21], whereas *hETV2*-overexpressed organoids [16] lacked *EOMES*. Because IPC is believed to contribute to cortical expansion in primates [42, 43], the upregulation of *EOMES* at 65 days possibly induced organoid expansion. Concordantly, Shi et al. demonstrated a rapid expansion in the size of organoids induced by vascularization around 65–70 days [21]. These findings support the importance of vascularization in neurogenesis in human cerebral organoids. However, it cannot be ruled out that these results may arise from differences in culture periods rather than the differences in vascularization protocols.

Next, to unbiasedly identify transcriptomic changes associated with vascularization, we comprehensively analyzed genes differentially expressed by vascularization in neuronal populations (Fig. 4C and Additional file 10: Table S3). The upregulated genes in *hETV2*-overexpressed organoid contained many homeodomain-containing transcription factors, such as *HOXA9*, *HOXA10*, *HOXB2*, *HOXB9*, *HOXC10*, and *MEIS2*, as observed in the previous analysis of all cell types. In organoids co-cultured with HUVEC, neuroid family genes such as *NEUROD2* and *NEUROD6*, which are proneural basic helix-loop-Helix (bHLH) transcription factors responsible for neuronal differentiation and specification [44], were significantly upregulated (Fig. 4C). These gene alterations were consistent with the upregulation of GO terms involved in “Neuron development” based on GSEA (Fig. 4D, left panel). Consistent with our finding that HUVEC co-culture enhanced EX proportions (Fig. 4A), *NEUROD2/6* is important for glutamatergic function in cortical neurons [45]. In addition, in organoid co-culture with HUVEC protocol, *SOX2* and long noncoding RNA *SOX2-OT* were downregulated in 65-day culture,

whereas only *SOX2-OT* was downregulated in 100-day culture protocols (Fig. 4C). Furthermore, *TCF7L2* was suppressed in *hETV2*-overexpressed and HUVEC co-cultured (65-day) organoids (Fig. 4C). Decreased expression of these genes has been linked to reduced Wnt activity and suppression of the proliferation of radial glial cells and intermediate progenitors [46]. Consistently, the proportion of *EOMES*⁺ IPCs was reduced by HUVEC co-culture from 13.6 to 11.0% in the 65-day culture and from 5.0 to 3.9% in the 100-day culture (Fig. 4A). GSEA analysis predicted that alterations in neurodevelopmental processes as well as downregulation of biological processes are involved in apoptosis in organoid neurons, irrespective of the vascularization protocols (Fig. 4B and Additional file 9: Fig. S7C). This indicates that vascularization generally prevents neuronal cell death. Altogether, these findings suggest that vascularization regulates the balance between neuronal cell differentiation and progenitor cell proliferation in cerebral organoids. However, understanding the underlying molecular mechanisms require further study.

Characterization of vascular-like cells that develop in human cerebral organoids

Finally, we focused on the VLC population, which are neither neural (*RBFOX3*⁺), proliferative (*TOP2A*⁺), nor glial cells (*GFAP*⁺, *AQP*⁺, and *OLIG2*⁺), expressing genes characteristic of mesodermal-derived cells (Fig. 1B). To further investigate these cells, we isolated them from the combined dataset (Fig. 5A). These cells expressed genes characteristic of cells that comprise blood vessels, such as *CLDN5*, *ACTA2*, *COL1A1*, and *RGS5* (Fig. 5B). The isolated cell population was re-clustered at a resolution of 0.3, yielding 11 clusters (Additional file 11: Fig. S8A). The resolution was determined using a “clustree” package in Seurat, illustrating the cluster relationships at multiple resolutions (0 to 1 in 0.1 increments) (Additional file 11: Fig. S8B). In detail, we used the clustering tree to guide selection of optimal clustering resolution *n* based on the following criteria: (1) greater number of branches branching from *n*–1 to *n* (because large differences are observed among clusters) and (2) fewer branches from *n* to *n* + 1 (because the number of clusters is stable after the optimal resolution). Cell types were assigned to these clusters according to GSEA based on the unbiasedly determined marker gene expression (Fig. 5C and Additional file 11: Fig. S8C, S8D). These cell types include vascular-like cells, such as ECs, fibroblasts, and mural cells (pericytes and smooth muscle cells).

The three endothelial-like (ECL) cell types, ECL, metallothionein-expressing ECL (M-ECL), hormone-regulating ECL (H-ECL), commonly expressed *CLDN5*, a component of brain endothelial-specific tight junctions

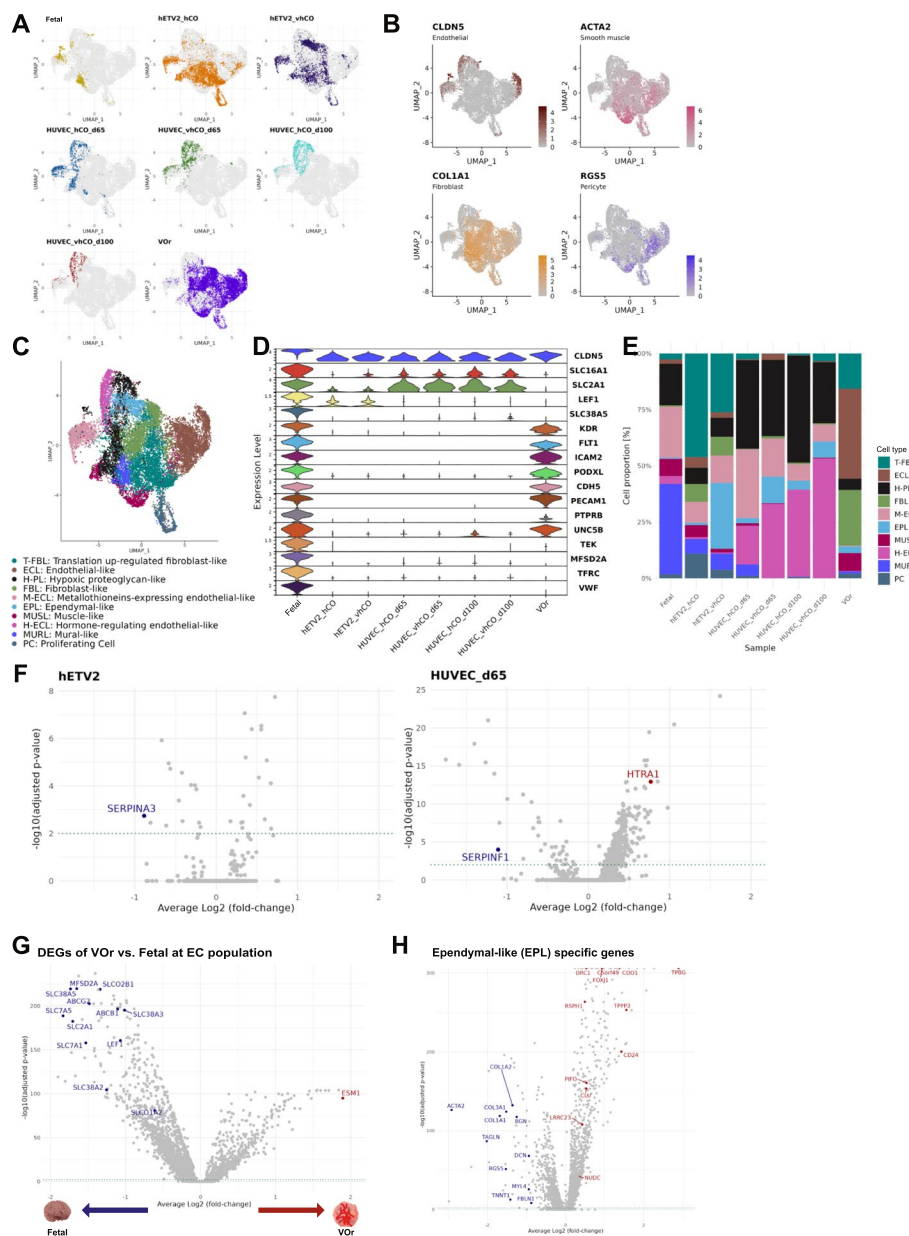


Fig. 5 Characterization of transcriptomic profile alterations with vascularization in vascular-related-like cell (VLC) subtypes. **A** UMAP for each sample of VLC. **B** Marker expression of vascular cells (*CLDN5*, endothelial cells; *ACTA2*, smooth muscle cells; *COL1A1*, fibroblast; *RG55*, pericytes). **C** UMAP assigned to cell types based on unbiased gene expression profiles [See Additional file 11: Fig. S8A for clusters to which cell types are assigned; Additional file 11: Fig. S8C and S8D show the annotation]. **D** Endothelial cell marker expression. **E** Proportion of cells in each subtype per sample. **F** Volcano plot of genes altered by vascularization in the *CLDN5*⁺ endothelial-like (ECL) cells. The data for organoids co-cultured with HUVECs for 100 days are not shown due to the low number of genes altered by vascularization. **G** Differentially expressed genes in VOr ECL cells (*CLDN5*⁺, *KDR*⁺, *FLT1*⁺) compared to endothelial cells in the fetal brain. The larger the averaged $\log_2(\text{FC})$, the more enriched in VOr, and vice versa. **H** Gene expression specific to an ependymal-like (EPL) cluster. Genes colored in red represent highly expressed genes in EPL compared to other clusters, and genes colored in blue represent less expressed genes

known as a robust EC marker (Fig. 5B, D) [9, 47]. M-ECL and H-ECL expressed unique transcriptomic profiles, such as metallothioneins and thyrotropin-releasing hormone (TRH), respectively, in addition to *CLDN5*.

Metallothionein contributes to the detoxification of excess heavy metals and the removal of reactive oxygen species, while TRH regulates hormone secretion in the brain [48, 49]. M-ECL and H-ECL were

present predominantly in cerebral organoids (*hETV2*-overexpressed and HUVEC co-cultured organoids) and the fetal brain (Fig. 5E). In contrast, VOr lacked M-ECL and H-ECL, but instead contained abundant ECL with the expression of *PECAMI* (protein: CD31) and *FLT1* (protein: VEGFR1), which are important for defining endothelial properties [9, 50, 51]. To further highlight the heterogeneity in ECL cells across different protocols, we characterized the expression of commonly referenced marker genes characteristic of cerebral vascular ECs. To achieve this, we extracted *CLDN5*⁺ ECL cells from all VLCs and profiled their marker genes (Fig. 5D). Genes encoding solute carrier proteins in human brain capillary ECs, such as *SLC16A1* and *SLC2A1*, are barely expressed in VOr [52]. Furthermore, *LEF1*, a transcription factor controlling the blood–brain barrier (BBB)-specific gene expression repertoire, is expressed only in the fetal brain and part of the cerebral organoids [53]. In contrast, *CLDN5*⁺ ECL cells in the cerebral organoids lacked the expression of *PECAMI* and VEGFRs (*KDR* and *FLT1*) (Fig. 5E). To ascertain whether vascularization in these cerebral organoids improves their ECL cell characteristics, we explored genes whose expression was significantly altered by vascularization in *CLDN5*⁺ ECL cells (Fig. 5F and Additional file 12: Table S4), which identified a few genes significantly altered by vascularization (Fig. 5F). On the contrary, several cerebrovascular-associated genes were significantly altered by vascularization in the *CLDN5*⁺ cell population. For example, the expression of *SERPINF1*, which belongs to the serpin family and has antiangiogenic activity [54], decreased in HUVEC co-cultured (65 days) organoids. Furthermore, in the *hETV2*-overexpressed organoid-derived *CLDN5*⁺ cell population, the expression of *SERPINA3*, which negatively regulates angiogenesis and inflammation, was reduced [55]. In addition, *HTRA1*, a causative gene for cerebral small-vessel disease [56, 57], was upregulated in HUVEC co-cultured (65 days) organoids. These findings suggest that ECL cells in cerebral organoids possess properties specific to cerebrovascular cells but lack sufficient properties as vascular ECs. Furthermore, vascularization may induce the expression of several gene profile characteristics of the cerebrovascular system. However, it may not lead to the acquisition of full EC properties for ECL cells. To characterize ECL cells in the VOr, we identified differentially expressed genes between *CLDN5*⁺ cells in the VOr and fetal brain ECs. The expression of *ESM1*, a protein synthesized and secreted by ECs in the lungs and kidneys, was elevated in VOr [58] (Fig. 5G and Additional file 13: Table S5). Conversely, the expression of BBB-related genes, such as a regulator of BBB permeability (*MSFDA2A*), BBB-specific efflux (*ABCB1* and *ABCG2*), and influx (*SLCO1A2* and *SLCO2B1*) transporters [59,

60] was reduced (Fig. 5G). These findings suggest that the *CLDN5*⁺ population of VOr expresses the core genes as real ECs but fails to reproduce the characteristics of cerebral blood vessels despite treatment with neurotropic reagents N2 and B2 at the late stage of maturation. Figure 5A also highlights that *CLDN5*⁺ population between fetal brain and VOr significantly differed, suggesting different gene expression profiles of *CLDN5*⁺ population in these samples. This difference might reflect the lack of cerebrovascular-specific genes in VOr.

To further check if pericytes express BBB-related genes, we sequestered MURL clusters that include pericytes. The MURL clusters included *RGSS5*⁺ population, which may be pericytes. We found that the MURL clusters expressed very few BBB-related genes in VOr, except for several genes (*SLC38A2* and *LEF1*) (Additional file 14: Fig. S9A and S9B).

We also found non-vascular cells in the VLCs, such as proliferating cells (PC) and ependymal-like cells. Ependymal cells in the human brain control cerebrospinal flow to efflux waste products [61]. To investigate the nature of the EPL in organoids in detail, we performed a differential expression test between the EPL cluster and the other clusters. The EPL showed enhanced expression of cilio-genesis-related genes (*TPBG*, *CDO1*, *CD240*, *DRC1*, and *C5orf49*) [62] and suppressed expression of perivascular-like cell marker genes (*COL1A1*, *ACTA2*, and *TAGLN*) (Fig. 5H and Additional file 15: Table S6). We also found that EPL upregulated *FOXJ1*, *CLU*, *PIFO*, *DYMLRB2*, *LRRRC23*, *RSPH1*, *TPPP3*, and *NUDC* (Fig. 5H), the marker genes of ependymal cells [63–65]. Moreover, the overexpression of *hETV2* remarkably increased the population of EPL. These results suggest that *hETV2* overexpression induces vasculogenesis as well as ependymal-like cell development.

Collectively, ECs could be present in organoids regardless of vascularization, whereas vascularization induced alterations in functional proteins in these cells. There is a trade-off relationship between the expression levels of genes critical to ECs (e.g., *PECAMI* and *FLT1*) and those expressed in a BBB-specific manner (e.g., *SLC2A1*), in which the balance of expression of both types of genes depends on vascular induction strategies.

Discussions

Various cerebral organoid vascularization strategies improve the survivability and reproducibility of cerebral organoids. The increasing volume of publicly available scRNA-seq datasets of human cerebral organoids has enabled comparative studies to identify generalizable trends and/or variability among individual studies. In this study, we systematically characterized the single-cell transcriptome of vascularized cerebral and vascular

organoids with induced cerebrovascular features. Our results reveal how vascular induction has transcriptomic effects on neuronal and vascular-like cell populations. We found several key findings in our analysis that they could not find from their individual previous studies. First, careful analysis of vascular-like cells revealed that BBB-related genes are expressed in vascular-like cells in the protocols in which neuronal cells and vascular-like cells are co-cultured for a certain period (Cakir et al.'s and Sun et al.'s studies). On the other hand, in the protocol in which neurotrophic factors were added to vascular organoids (Shi et al.'s study), vascular-like cells lacked BBB-related genes. However, the vascular organoids expressed more endothelial cell markers, including *PECAMI*, than the cerebral organoids. These findings suggest that the interaction between neurons and vascular-like cell populations is important for the cerebrovascular-specific profile of endothelial-like cells. Second, our data revealed the presence of cell populations unique to the protocol (i.e., microglia and ependymal cells). It was shown that only vascular organoids expressed microglia-like cells, indicating a possible achievement of immunization. Nevertheless, it is still a problem that microglia-like cells in the vascular organoids may not express enough identity as genuine microglia and that the populations are very small. These results emphasize that we need to revisit not only vascularization, but immunization as well. Furthermore, it was shown that *hETV2* overexpression protocol generates ependymal-like cells. Although these observations have already been noted in the individual previous studies, it is noteworthy that we found no such cell populations in the other protocols. Based on the above two insights, in order to achieve the generation of vascularized cerebral organoids with higher fidelity, for example, one can fuse vascular and cerebral organoids and culture the resulting assembloid for a long period of time.

This study has several limitations. First, the supplements used to generate the organoids differ among protocols. Heparin, included in Shi et al.'s protocol but not in Cakir et al.'s, can induce pluripotent stem cells into neurons but also promote early mesoderm induction [66]. Insulin, included in Cakir et al.'s protocol but not in Shi et al.'s, promotes both neuronal maturation and blood vessel development [67]. We cannot rule out the possibility that these supplements may be confounding factors in vascularization. Second, the duration of cultivation also differs among protocols. The scRNA-seq data that we used were derived from organoids at 70 days for the Cakir et al.'s protocol, 65 and 100 days for the Shi et al.'s protocol, and 40 days for the Sun et al.'s protocol. Therefore, comparing vascularization methods at the same time point is a challenge for the future. Third, the vascular organoids from Sun et al.'s

protocol does not assemble with the cerebral organoids and this dataset lacks the ectoderm-derived cell population. Therefore, it is impossible to analyze the effects of induced blood vessels on neuronal cells in the assembloid.

Although this study has several limitations mentioned above, our data provide important insights into future strategies for vascularization of cerebral organoids. This study showed that characteristics in vascular-like cells have protocol-dependent pros and cons and that microglia and ependymal cells are induced but have not acquired sufficient identities. However, it was also shown that the presence of vasculature, regardless of protocol, can improve the gene expression profile of organoid cells. Overall, the benchmarks we constructed suggest that diverse vascularization strategies have issues that need to be resolved. In future studies, detailed analysis of the induced vasculature using techniques such as spatial transcriptomics and vasculature-targeted scRNA-seq will be required to precisely evaluate vascular cell types and their functional aspects. Furthermore, the batch effect may not have been fully eliminated because we reanalyze sequence data from different laboratories.

Conclusions

Recent progress in scRNA-seq data analysis has enabled integrative comparisons of human cerebral organoids [28, 68]. Various studies have proposed methods for vascularizing human cerebral organoids, and several review articles have compared these methods. However, there has been no discussion on a data-driven comparison that can discover heterogeneity in vascularized organoids across protocols. Our new findings reveal that different vascularization methods contribute to different levels of heterogeneity, providing important knowledge for the utilization of vascularized organoids.

Methods

Data collection

We collected the FASTQ or BAM-formatted files from the NCBI Short Read Archive for the 10×Genomics platform. The downloaded files were converted to FASTQ files using “fastq-dump” (v2.11.0) or “bamtofastq” (v1.3.2). The FASTQ files were mapped to the human reference genome (GRCh38, v1.2.0) using the Cell Ranger count function (v6.0.1) with the default parameters [69]. Multiple sequences in the same experiment were pooled using the “aggr” function of Cell Ranger. For samples without 10×Genomics platform data, we obtained post-mapped cell-gene matrices from the Gene Expression Omnibus (GEO) database.

Pre-processing

We quality-controlled the cell-gene matrix output from the Cell Ranger analysis pipeline named “filtered_feature_bc_matrix” to exclude low-quality cells. Low-quality cells exhibited (1) high mitochondrial expression, (2) low feature mRNA expression, or (3) multiplet profiles [61]. Therefore, we excluded low-quality cells from the scRNA-seq libraries of cerebral and vascularized cerebral organoids and fetal brain under the following conditions: (1) organoid, >5%; fetal brain, >10%; and (2) less than 1000 feature genes. We set the cutoff value of the fraction of mitochondrial counts per cell (mtDNA%) in fetal brain at 10%, instead of 5%, because Osorio et al. concluded that the mtDNA% of human tissues is generally high and thus the cutoff value should be >10% [70]. A multiplet is defined as an artificial single-cell profile produced by two or more cells containing the same barcode. To filter the multiplets, we predicted and eliminated multiplets using Single-Cell Remover of Doublets (Scrublet v0.2.3) with default parameters [71].

Data integration

Pre-processed matrices from multiple samples were integrated and clustered using Seurat (v4.0) in R (v4.1.3) environment [72]. Variations in technical factors, including the sequencing depth in samples obtained from different experiments, lead to batch effects [73]. To eliminate this variation, we used the “SCTransform” function to normalize and variance-stabilize gene counts. Next, feature genes for integration were selected using the “SelectIntegrationFeatures” function and normalized by the “PrepSCTIntegration” function. Then, we identified the integration anchors of all sample data using the “FindIntegrationAnchors” function and integrated all assays with these anchors using the “IntegrateData” function. The integrated gene expression was compressed to 30 dimensions using the “RunPCA” function, and then the feature genes from 1 to 20 dimensions were k-mer clustered using the “FindNeighbors” and “FindClusters” functions. The compression dimensions were selected using the “ElbowPlot” function (Additional file 14: Fig. S9C).

Cell type determination

Cell types were determined using the following steps: (1) normalization and scaling, (2) dimensionality reduction, (3) clustering, and (4) cell type assignment using marker genes for each sample. These processes were performed differently from the “Data Integration” process to correctly assign cell types in the sample even under varying profiles among samples. The determined cell types were represented one-to-one with cell barcodes for use

in all subsequent analyses. Each step was implemented according to Seurat’s Vignette by normalization and scaling with the “SCTransform” function, PCA and UMAP dimensionality reduction from 1 to 20 dimensions, clustering with “FindNeighbors” and “FindClusters,” and cell type determination using the reported marker genes.

Differentially expressed gene analysis

To capture changes in gene expression profiles, gene sets varying among two conditions (e.g., vascularized organoid and fetal brain) were identified by the Wilcoxon rank sum test using the “FindMarker” function in the Seurat package. The “FindMarker” function was implemented with the target condition (ident.1 parameter) and the comparison condition (ident.2 parameter). From the calculated genes, only gene sets satisfying the condition (adjusted p -values with Bonferroni correction) < 0.01 were extracted and used in the subsequent analysis, except for volcano plots. Volcano plots were plotted as average \log_2 FC on the x -axis and $-\log_2$ (adjusted p -value) on the y -axis with full gene sets. Among the gene sets of interest, upregulated genes are highlighted in red, and downregulated genes are highlighted in blue. In addition, a threshold line (adjusted p -value < 0.01) is represented by the green dotted line.

Sample correlation with cell type

To determine the genetic similarity of human cerebral organoids to the fetal brain, we calculated the correlations of unbiased marker genes in each cell type of each organoid and fetal brain. First, we calculated marker genes, which are cell type-specific upregulated genes, with the Wilcoxon rank sum test using the “FindMarker” function in the Seurat package (see “Differentially expressed gene analysis”). Then, we calculated Pearson’s correlations for \log_2 FC of marker genes under (adjusted p -values with Bonferroni correction) < 0.01 to define similarity.

Gene set enrichment analysis (GSEA)

We performed GSEA to predict biological processes from differentially expressed genes (see “Differentially expressed gene analysis”) using the “clusterProfiler” package (v4.2.2) in the R environment [74]. First, we predicted pathways using a “gseGO” function with default parameters under the condition (adjusted p -values with Bonferroni correction) < 0.01. Second, we computed the similarity matrix between GO terms using the “pairwise_termsim” function of the “enrichplot” package (v1.14.2) and visualized gene sets as a network using the “emaplot” function. The color range was determined by the enrichment score, which indicated the predicted variability of each term.

Pseudotime analysis

To determine the changes in gene expression during the differentiation time course, cell trajectory lineages and differentiation pseudotime were calculated using the slingshot package (v2.2.0) [75]. The 2D UMAP coordinate matrix was extracted from the integrated Seurat object to execute a trajectory of slingshot analysis with all Seurat clusters and the root cluster number as the input. The root cell cluster was defined as *TOP2A*⁺ proliferating cells with the highest expression of *SOX2*. A minimum spanning tree on the cluster is constructed by the “getLineages” function to identify the phylogenetic relationships across the cluster. We then inferred the pseudotimes by fitting the principal curves using the “getCurves” function. The calculated pseudotimes were averaged using the “averagePseudotime” function of the “TrajectoryUtils” package to calculate the pseudotime at each lineage.

Gene expression along the pseudotime course

To characterize differences in gene expression during differentiation progression, we plotted gene expression along the pseudotime on a differentiation trajectory. The pseudotime was calculated by trajectory analysis using a slingshot and then averaged for each differentiation trajectory. Gene expression along the pseudotime was fitted by a loess approximation using the “geom_stat” function in the ggplot2 package (v 3.3.6).

Abbreviations

BBB	Blood-brain barrier
EC	Endothelial cells
EPL	Ependymal-like
FC	Fold-change
GSEA	Gene set enrichment analysis
HUVEC	Human umbilical vein endothelial cells
IN	Inhibitory neuron
IPC	Intermediate progenitor cell
VLC	Vascular-related-like cell
OPC	Oligodendrocyte precursor cells
PC	Proliferating cell
TRH	Thyrotropin-releasing Hormone
UMAP	Uniform Manifold Approximation and Projection
UPRC	Unfolded protein response cells

Supplementary Information

The online version contains supplementary material available at <https://doi.org/10.1186/s12915-023-01711-1>.

Additional file 1: Fig. S1. The pre-processing of multiple scRNA-seq data. (A) Analysis method overview. Cell types were individually assigned and integrated for intravascular organoids, non-vascular organoids, and fetal brains collected from public databases. (B) Parameters for each sample. Left panel: amount of characteristic RNA expression; middle panel: total RNA expression; right panel: mitochondrial expression.

Additional file 2: Fig. S2. Characteristic gene expression profiles of annotated cell types. (A-H) Expression of marker genes corresponding to cell types in each sample.

Additional file 3: Fig. S3. Integration of scRNA-seq data. (A) Clusters of integrated samples. (B) UMAP for each integrated sample. (C) UMAP indicating cell types in each integrated sample. (D) Expression of each marker gene.

Additional file 4: Fig. S4. Evidence for cell type annotation. (A) Annotation tree indicating the cell type assignment strategy. If there is no expression of the indicated marker gene, follow the path of “Negative” to be a candidate for the cell type below. (B) The overlap of the top 100 genes expressed in each cell type is represented in Upset plot. To statistically assess the independence of the overlap of the top 100 genes in any two cell types, statistical analysis was performed by Fisher’s exact test with Bonferroni’s correction. Adjusted *p*-values up to four decimal places are shown next to the Upset plot. There are some cell types that have been determined not to be statistically independent of one another, such as IPC vs. OPC in the fetal brain. However, actual number of genes that overlap between IPC and OPC of fetal brain is only five, suggesting that the overlap of the top genes of these two cell types is quite small.

Additional file 5: Fig. S5. scRNA-seq data analysis in ectoderm cell subtypes. (A) Overlap of characteristic genes for each cell type between each organoid and corresponding to the fetal brain. Differentially expressed genes specific to each cell group were identified with a cut-off at corrected *p*-value. The genes overlapping with the Venn diagram were plotted using the “ggvenn” package (v0.1.9). (B) Cell counts for each cell type in each sample. (C) Dot plot of expression of microglial markers in VOR samples.

Additional file 6: Table S1. Genes commonly upregulated by vascularization and their corrected *p*-values and average log₂-fold changes are listed. The “upregulated” tab lists commonly upregulated genes and the “downregulated” tab lists commonly downregulated genes.

Additional file 7: Fig. S6. GO terms altered by vascularization. Plot of the differential expression levels of the gene sets characteristic of each GO term, visualized by the “heatmap” function of the “enrichplot” package (v1.16.2). The “ENTREZID” were converted to gene symbols using the “setReadable” function of the “DOSE” package (v3.22.1).

Additional file 8: Table S2. List of genes altered by vascularization. No cut-off *p*-values are used in this table.

Additional file 9: Fig. S7. Integration and downstream analysis of neuronal subtypes. (A) UMAP in each sample of extracted neurons (IPC, EX, IN). (B) Differentiation trajectories of ectodermal cells revealed by trajectory analysis. (C) Alterations in GO-terms induced by vascularization in neurons. Note that color indicates enrichment score, not *p*-value.

Additional file 10: Table S3. List of genes altered by vascularization in neuronal populations. No cut-off *p*-values are used in this table.

Additional file 11: Fig. S8. Evidence for determination of VLC subtypes. (A) Eleven clusters of resolution = 0.3 obtained unbiased. The resolution was determined by the “clustree” shown in S8B Fig. For each cluster, a cell type was assigned based on the evidence in S8C and S8D Fig. (B) Clustree plot representing cluster relationships at resolutions from 0.1 to 1 (step 0.1) using the “clustree” package (v0.5.0). The dot size indicates the number of cells, and the line extending from the cluster indicates the cluster relationship. (C) Expression levels of genes that were characteristically expressed in each cluster. The color of the plots matches the concept color of each cell type. (D) GSEA results calculated based on non-biased computed gene sets. The table on the right side presents the *p*-value for each GO term. The plots were generated by the “gseaplot2” function of the “enrichplot” package.

Additional file 12: Table S4. List of genes altered by vascularization in endothelial populations. No cut-off *p*-values are used in this table.

Additional file 13: Table S5. Differentially expressed genes in the fetal brain of endothelial populations. No cut-off *p*-values are used in this table.

Additional file 14: Fig. S9. BBB-related genes and cluster determination. (A) Feature plot of BBB-related genes expression in pericyte-like clusters. (B) Violin plot of BBB-related genes expression in pericyte-like clusters. (C) Plot of standard deviation for each feature dimension to select the feature dimension with the smallest change in standard deviation.

Additional file 15: Table S6. Differentially expressed genes were specifically expressed for each cluster in the VLC population. No cut-off *p*-values are used in this table.

Acknowledgements

We thank H. Noguchi, A. Kawamura, K. Hashimoto, S. Aoki, K. Hirata and R. Sanno for server construction for the analysis.

Authors' contributions

Conceptualization: Y.S. and K. K.; data curation: Y. S.; formal analysis: Y.S.; funding acquisition: K.K. and T. A.; investigation: Y.S. and K. K.; methodology: Y. S.; project administration: K.K.; software: Y.S.; supervision: K. K. and T. A.; validation: K. K.; visualization: Y. S.; writing—original draft: Y. S. and K. K.; writing—review and editing: Y. S. and K. K. All authors read and approved the final manuscript.

Funding

This study was supported by grants from JSPS KAKENHI (19K20196 and 22K17815 to KK).

Availability of data and materials

All data generated or analyzed during this study are included in this published article, its supplementary information files and publicly available repositories. The data from Cakir's study (*hETV2*), Shi's study (*HUVEC*), and Sun's study (*VO*) have been deposited in the Sequence Read Archive [BioProject: PRJNA553561, PRJNA542649, PRJNA764860] (<https://www.ncbi.nlm.nih.gov/bioproject/PRJNA553561>, <https://www.ncbi.nlm.nih.gov/bioproject/PRJNA542649>, <https://www.ncbi.nlm.nih.gov/bioproject/PRJNA764860>), respectively. The human fetal brain data have been deposited in the Gene Expression Omnibus [GSE: GSE162170] (<https://www.ncbi.nlm.nih.gov/geo/query/acc.cgi?acc=GSE162170>). Requests for material should be made to the corresponding authors.

Declarations

Ethics approval and consent to participate

Not applicable.

Consent for publication

Not applicable.

Competing interests

The authors declare that they have no competing interests.

Received: 24 March 2023 Accepted: 25 September 2023

Published online: 09 November 2023

References

- Lancaster MA, Renner M, Martin CA, Wenzel D, Bicknell LS, Hurler ME, et al. Cerebral organoids model human brain development and microcephaly. *Nature*. 2013;501:373–9. <https://doi.org/10.1038/nature12517>.
- Pellegrini L, Albecka A, Mallery DL, Kellner MJ, Paul D, Carter AP, et al. SARS-CoV-2 infects the brain choroid plexus and disrupts the blood-CSF barrier in human brain organoids. *Cell Stem Cell*. 2020;27:951–961.e5. <https://doi.org/10.1016/j.stem.2020.10.001>.
- Ramani A, Müller L, Ostermann PN, Gabriel E, Abida-Islam P, Müller-Schiffmann A, et al. SARS-CoV-2 targets neurons of 3D human brain organoids. *EMBO J*. 2020;39: e106230. <https://doi.org/10.15252/embj.2020106230>.
- Yu J. Vascularized organoids: a more complete model. *Int J Stem Cells*. 2021;14:127–37. <https://doi.org/10.15283/ijsc.20143>.
- Matsui TK, Tsuru Y, Hasegawa K, Kuwako KI. Vascularization of human brain organoids. *Stem Cells*. 2021;39:1017–24. <https://doi.org/10.1002/stem.3368>.
- Shen Q, Goderie SK, Jin L, Karanth N, Sun Y, Abramova N, et al. Endothelial cells stimulate self-renewal and expand neurogenesis of neural stem cells. *Science*. 2004;304:1338–40. <https://doi.org/10.1126/science.1095505>.
- Ross JM, Kim C, Allen D, Crouch EE, Narsinh K, Cooke DL, et al. The expanding cell diversity of the brain vasculature. *Front Physiol*. 2020;11: 600767. <https://doi.org/10.3389/fphys.2020.600767>.
- Sweeney MD, Zhao Z, Montagne A, Nelson AR, Zlokovic BV. Blood-brain barrier: from physiology to disease and back. *Physiol Rev*. 2019;99:21–78. <https://doi.org/10.1152/physrev.00050.2017>.
- Winkler EA, Kim CN, Ross JM, Garcia JH, Gil E, Oh I, et al. A single-cell atlas of the normal and malformed human brain vasculature. *Science*. 2022;375:eabi7377. <https://doi.org/10.1126/science.abi7377>.
- Paredes I, Himmels P, de Almodóvar CR. Neurovascular communication during CNS development. *Dev Cell*. 2018;45:10–32. <https://doi.org/10.1016/j.devcel.2018.01.023>.
- Snappyan M, Lemasson M, Brill MS, Blais M, Massouh M, Ninkovic J, et al. Vasculature guides migrating neuronal precursors in the adult mammalian forebrain via brain-derived neurotrophic factor signaling. *J Neurosci*. 2009;29:4172–88. <https://doi.org/10.1523/JNEUROSCI.4956-08.2009>.
- Won C, Lin Z, Kumar TP, Li S, Ding L, Elkhali A, et al. Autonomous vascular networks synchronize GABA neuron migration in the embryonic forebrain. *Nat Commun*. 2013;4:2149. <https://doi.org/10.1038/ncomms3149>.
- Tsai HH, Niu J, Munji R, Davalos D, Chang J, Zhang H, et al. Oligodendrocyte precursors migrate along vasculature in the developing nervous system. *Science*. 2016;351:379–84. <https://doi.org/10.1126/science.aad3839>.
- Mansour AA, Gonçalves JT, Bloyd CW, Li H, Fernandes S, Quang D, et al. An in vivo model of functional and vascularized human brain organoids. *Nat Biotechnol*. 2018;36:432–41. <https://doi.org/10.1038/nbt.4127>.
- Daviaud N, Friedel RH, Zou H. Vascularization and engraftment of transplanted human cerebral organoids in mouse cortex. *eNeuro*. 2018;5. <https://doi.org/10.1523/ENEURO.0219-18.2018>.
- Cakir B, Xiang Y, Tanaka Y, Kural MH, Parent M, Kang YJ, et al. Engineering of human brain organoids with a functional vascular-like system. *Nat Methods*. 2019;16:1169–75. <https://doi.org/10.1038/s41592-019-0586-5>.
- Ham Q, Jin YB, Kim J, Lee MO. Blood vessel formation in cerebral organoids formed from human embryonic stem cells. *Biochem Biophys Res Commun*. 2020;521:84–90. <https://doi.org/10.1016/j.bbrc.2019.10.079>.
- Morita R, Suzuki M, Kasahara H, Shimizu N, Shichita T, Sekiya T, et al. ETS transcription factor ETV2 directly converts human fibroblasts into functional endothelial cells. *Proc Natl Acad Sci U S A*. 2015;112:160–5. <https://doi.org/10.1073/pnas.1413234112>.
- Li J, Zhu Y, Li N, Wu T, Zheng X, Heng BC, et al. Upregulation of ETV2 expression promotes endothelial differentiation of human dental pulp stem cells. *Cell Transplant*. 2021;30:963689720978739. <https://doi.org/10.1177/0963689720978739>.
- Kim JJ, Kim DH, Lee JY, Lee BC, Kang I, Kook MG, et al. CAMP/EPAC signaling enables ETV2 to induce endothelial cells with high angiogenesis potential. *Mol Ther*. 2020;28:466–78. <https://doi.org/10.1016/j.jymth.2019.11.019>.
- Shi Y, Sun L, Wang M, Liu J, Zhong S, Li R, et al. Vascularized human cortical organoids (vOrganoids) model cortical development in vivo. *PLOS Biol*. 2020;18: e3000705. <https://doi.org/10.1371/journal.pbio.3000705>.
- Pham MT, Pollock KM, Rose MD, Cary WA, Stewart HR, Zhou P, et al. Generation of human vascularized brain organoids. *NeuroReport*. 2018;29:588–93. <https://doi.org/10.1097/WNR.0000000000001014>.
- Takebe T, Sekine K, Enomura M, Koike H, Kimura M, Ogaeri T, et al. Vascularized and functional human liver from an iPSC-derived organ bud transplant. *Nature*. 2013;499:481–4. <https://doi.org/10.1038/nature12271>.
- Sun XY, Ju XC, Li Y, Zeng PM, Wu J, Zhou YY, et al. Generation of vascularized brain organoids to study neurovascular interactions. *Life*. 2022;11:e76707. <https://doi.org/10.7554/eLife.76707>.
- Song L, Yuan X, Jones Z, Griffin K, Zhou Y, Ma T, et al. Assembly of human stem cell-derived cortical spheroids and vascular spheroids to model 3-D brain-like tissues. *Sci Rep*. 2019;9:5977. <https://doi.org/10.1038/s41598-019-42439-9>.
- Aird WC. Phenotypic heterogeneity of the endothelium: I. Structure, function, and mechanisms. *Circ Res*. 2007;100:158–73. <https://doi.org/10.1161/01.RES.0000255691.76142.4a>.
- Trevino AE, Müller F, Andersen J, Sundaram L, Kathiria A, Shcherbina A, et al. Chromatin and gene-regulatory dynamics of the developing human cerebral cortex at single-cell resolution. *Cell*. 2021;184:5053–5069.e23. <https://doi.org/10.1016/j.cell.2021.07.039>.
- Velasco S, Kedaigle AJ, Simmons SK, Nash A, Rocha M, Quadrato G, et al. Individual brain organoids reproducibly form cell diversity of the human cerebral cortex. *Nature*. 2019;570:523–7. <https://doi.org/10.1038/s41586-019-1289-x>.
- Quadrato G, Nguyen T, Macosko EZ, Sherwood JL, Min Yang S, Berger DR, et al. Cell diversity and network dynamics in photosensitive human brain organoids. *Nature*. 2017;545:48–53. <https://doi.org/10.1038/nature22047>.

30. Ormel PR, de Sá RV, van Bodegraven EJ, Karst H, Harschnitz O, Sneeboer MAM, et al. Microglia innately develop within cerebral organoids. *Nat Commun*. 2018;9:4167. <https://doi.org/10.1038/s41467-018-06684-2>.
31. Cakir B, Park IH. Getting the right cells. *Life*. 2022;11:e80373. <https://doi.org/10.7554/eLife.80373>.
32. Göcz B, Takács S, Skrapits K, Rumpel É, Solymosi N, Pólska S, et al. Estrogen differentially regulates transcriptional landscapes of preoptic and arcuate kisspeptin neuron populations. *Front Endocrinol (Lausanne)*. 2022;13: 960769. <https://doi.org/10.3389/fendo.2022.960769>.
33. Rumpansuwon K, Prommahom A, Dharmasaroja P. eEF1A2 knockdown impairs neuronal proliferation and inhibits neurite outgrowth of differentiating neurons. *NeuroReport*. 2022;33:336–44. <https://doi.org/10.1097/WNR.0000000000001791>.
34. Chung D, Shum A, Caraveo G. GAP-43 and BASP1 in axon regeneration: Implications for the treatment of neurodegenerative diseases. *Front Cell Dev Biol*. 2020;8: 567537. <https://doi.org/10.3389/fcell.2020.567537>.
35. Salehpour F, Mahmoudi J, Kamari F, Sadigh-Eteghad S, Rasta SH, Hamblin MR. Brain photobiomodulation therapy: a narrative review. *Mol Neurobiol*. 2018;55:6601–36. <https://doi.org/10.1007/s12035-017-0852-4>.
36. Cheng Y, Loh YP, Birch NP. Neuroserpin attenuates H2O2-induced oxidative stress in hippocampal neurons via AKT and BCL-2 signaling pathways. *J Mol Neurosci*. 2017;61:123–31. <https://doi.org/10.1007/s12031-016-0807-7>.
37. Xu L, Xu Q, Xu F, Zhang W, Chen Q, Wu H, et al. MicroRNA-325-3p prevents sevoflurane-induced learning and memory impairment by inhibiting Nupr1 and C/EBPβ/IGFBP5 signaling in rats. *Aging (Albany NY)*. 2020;12:5209–20. <https://doi.org/10.18632/aging.102942>.
38. Veldman MB, Zhao C, Gomez GA, Lindgren AG, Huang H, Yang H, et al. Transdifferentiation of fast skeletal muscle into functional endothelium in vivo by transcription factor Etv2. *PLOS Biol*. 2013;11: e1001590. <https://doi.org/10.1371/journal.pbio.1001590>.
39. Kanton S, Boyle MJ, He Z, Santel M, Weigert A, Sanchís-Calleja F, et al. Organoid single-cell genomic atlas uncovers human-specific features of brain development. *Nature*. 2019;574:418–22. <https://doi.org/10.1038/s41586-019-1654-9>.
40. Noctor SC, Martínez-Cerdeño V, Ivic L, Kriegstein AR. Cortical neurons arise in symmetric and asymmetric division zones and migrate through specific phases. *Nat Neurosci*. 2004;7:136–44. <https://doi.org/10.1038/nn1172>.
41. Hevner RF. Intermediate progenitors and Tbr2 in cortical development. *J Anat*. 2019;235:616–25. <https://doi.org/10.1111/joa.12939>.
42. Pontious A, Kowalczyk T, Englund C, Hevner RF. Role of intermediate progenitor cells in cerebral cortex development. *Dev Neurosci*. 2008;30:24–32. <https://doi.org/10.1159/000109848>.
43. Martínez-Cerdeño V, Noctor SC, Kriegstein AR. The role of intermediate progenitor cells in the evolutionary expansion of the cerebral cortex. *Cereb Cortex*. 2006;16(Suppl 1):i52–61. <https://doi.org/10.1093/cercor/bhk017>.
44. Tutukova S, Tarabykin V, Hernandez-Miranda LR. The role of Neurod genes in brain development, function, and disease. *Front Mol Neurosci*. 2021;14: 662774. <https://doi.org/10.3389/fnmol.2021.662774>.
45. Bormuth I, Yan K, Yonemasu T, Gummert M, Zhang M, Wichert S, et al. Neuronal basic helix-loop-helix proteins Neurod2/6 regulate cortical commissure formation before midline interactions. *J Neurosci*. 2013;33:641–51. <https://doi.org/10.1523/JNEUROSCI.0899-12.2013>.
46. Chodelkova O, Masek J, Korinek V, Kozmik Z, Machon O. Tcf7L2 is essential for neurogenesis in the developing mouse neocortex. *Neural Dev*. 2018;13:8. <https://doi.org/10.1186/s13064-018-0107-8>.
47. Ma SC, Li Q, Peng JY, Zhouwen JL, Diao JF, Niu JX, et al. Claudin-5 regulates blood-brain barrier permeability by modifying brain microvascular endothelial cell proliferation, migration, and adhesion to prevent lung cancer metastasis. *CNS Neurosci Ther*. 2017;23:947–60. <https://doi.org/10.1111/cns.12764>.
48. Atrian S, Capdevila M. Metallothionein-protein interactions. *Biomol Concepts*. 2013;4:143–60. <https://doi.org/10.1515/bmc-2012-0049>.
49. Monga V, Meena CL, Kaur N, Jain R. Chemistry and biology of thyrotropin-releasing hormone (TRH) and its analogs. *Curr Med Chem*. 2008;15:2718–33. <https://doi.org/10.2174/092986708786242912https://www.ncbi.nlm.nih.gov/pubmed/18991632>.
50. Garcia FJ, Sun N, Lee H, Godlewski B, Mathys H, Galani K, et al. Single-cell dissection of the human brain vasculature. *Nature*. 2022;603:893–9. <https://doi.org/10.1038/s41586-022-04521-7>.
51. Jeong HW, Diéguez-Hurtado R, Arf H, Song J, Park H, Kruse K, et al. Single-cell transcriptomics reveals functionally specialized vascular endothelium in brain. *eLife*. 2022;11:e57520. <https://doi.org/10.7554/eLife.57520>.
52. Liebner S, Corada M, Bangsow T, Babbage J, Taddei A, Czupalla CJ, et al. Wnt/beta-catenin signaling controls development of the blood-brain barrier. *J Cell Biol*. 2008;183:409–17. <https://doi.org/10.1083/jcb.200806024>.
53. Roudnicky F, Kim BK, Lan Y, Schmucki R, Küppers V, Christensen K, et al. Identification of a combination of transcription factors that synergistically increases endothelial cell barrier resistance. *Sci Rep*. 2020;10:3886. <https://doi.org/10.1038/s41598-020-60688-x>.
54. Huang Q, Wang S, Sorenson CM, Sheibani N. PEDF-deficient mice exhibit an enhanced rate of retinal vascular expansion and are more sensitive to hyperoxia-mediated vessel obliteration. *Exp Eye Res*. 2008;87:226–41. <https://doi.org/10.1016/j.exer.2008.06.003>.
55. Sánchez-Navarro A, González-Soria I, Caldiño-Bohn R, Bobadilla NA. An integrative view of serpins in health and disease: The contribution of SerpinA3. *Am J Physiol Cell Physiol*. 2021;320:C106–18. <https://doi.org/10.1152/ajpcell.00366.2020>.
56. Oluwole OJ, Ibrahim H, Garozzo D, Hamouda KB, Hassan SIM, Hegazy AM, et al. Cerebral small vessel disease due to a unique heterozygous HTRA1 mutation in an African man. *Neurol Genet*. 2020;6:382. <https://doi.org/10.1212/NXG.0000000000000382>.
57. Uemura M, Nozaki H, Kato T, Koyama A, Sakai N, Ando S, et al. HTRA1-related cerebral small vessel disease: A review of the literature. *Front Neurol*. 2020;11:545. <https://doi.org/10.3389/fneur.2020.00545>.
58. Leroy X, Aubert S, Zini L, Franquet H, Kervoaze G, Villers A, et al. Vascular endocan (ESM-1) is markedly overexpressed in clear cell renal cell carcinoma. *Histopathology*. 2010;56:180–7. <https://doi.org/10.1111/j.1365-2559.2009.03458.x>.
59. Cui Y, Wang Y, Song X, Ning H, Zhang Y, Teng Y, et al. Brain endothelial PTEN/AKT/NEDD4-2/MFSD2A axis regulates blood-brain barrier permeability. *Cell Rep*. 2021;36: 109327. <https://doi.org/10.1016/j.celrep.2021.109327>.
60. Strazielle N, Ghersi-Egea JF. Efflux transporters in blood-brain interfaces of the developing brain. *Front Neurosci*. 2015;9:21. <https://doi.org/10.3389/fnins.2015.00021>.
61. Seo JS, Mantas I, Svenningsson P, Greenberg P. Ependymal cells-CSF flow regulates stress-induced depression. *Mol Psychiatry*. 2021;26:7308–15. <https://doi.org/10.1038/s41380-021-01202-1>.
62. Shah PT, Stratton JA, Stykel MG, Abbasi S, Sharma S, Mayr KA, et al. Single-cell transcriptomics and fate mapping of ependymal cells reveals an absence of neural stem cell function. *Cell*. 2018;173:1045–1057.e9. <https://doi.org/10.1016/j.cell.2018.03.063>.
63. Jacquet BV, Salinas-Mondragon R, Liang H, Therit B, Buie JD, Dykstra M, et al. FoxJ1-dependent gene expression is required for differentiation of radial glia into ependymal cells and a subset of astrocytes in the postnatal brain. *Development*. 2009;136:4021–31. <https://doi.org/10.1242/dev.041129>.
64. Cunin P, Beauvillain C, Miot C, Augusto JF, Preisser L, Blanchard S, et al. Clusterin facilitates apoptotic cell clearance and prevents apoptotic cell-induced autoimmune responses. *Cell Death Dis*. 2016;7: e2215. <https://doi.org/10.1038/cddis.2016.113>.
65. MacDonald A, Lu B, Caron M, Caporicci-Dinucci N, Hatrock D, Petrecca K, et al. Single cell transcriptomics of ependymal cells across age, region and species reveals cilia-related and metal ion regulatory roles as major conserved ependymal cell functions. *Front Cell Neurosci*. 2021;15: 703951. <https://doi.org/10.3389/fncel.2021.703951>.
66. Grunz H, McKeenan WL, Knöchel W, Born J, Tiedemann H, Tiedemann H. Induction of mesodermal tissues by acidic and basic heparin binding growth factors. *Cell Differ*. 1988;22:183–9. [https://doi.org/10.1016/0045-6039\(88\)90010-3](https://doi.org/10.1016/0045-6039(88)90010-3).
67. Chiu S-L, Cline HT. Insulin receptor signaling in the development of neuronal structure and function. *Neural Dev*. 2010;5:7. <https://doi.org/10.1186/1749-8104-5-7>.
68. Tanaka Y, Cakir B, Xiang Y, Sullivan GJ, Park I-H. Synthetic analyses of single-cell transcriptomes from multiple brain organoids and fetal brain. *Cell Rep*. 2020;30:1682–1689.e3. <https://doi.org/10.1016/j.celrep.2020.01.038>.
69. Zheng GX, Terry JM, Belgrader P, Ryvkin P, Bent ZW, Wilson R, et al. Massively parallel digital transcriptional profiling of single cells. *Nat Commun*. 2017;8:14049. <https://doi.org/10.1038/ncomms14049>.

70. Osorio D, Cai JJ. Systematic determination of the mitochondrial proportion in human and mice tissues for single-cell RNA-sequencing data quality control. *Bioinformatics*. 2021;37:963–7. <https://doi.org/10.1093/bioinformatics/btaa751>.
71. Wolock SL, Lopez R, Klein AM. Scrublet: Computational identification of cell Doublets in Single-cell transcriptomic data. *Cell Syst*. 2019;8:281–291. e9. <https://doi.org/10.1016/j.cels.2018.11.005>.
72. Hao Y, Hao S, Andersen-Nissen E, Mauck WM 3rd, Zheng S, Butler A, et al. Integrated analysis of multimodal single-cell data. *Cell*. 2021;184:3573–3587.e29. <https://doi.org/10.1016/j.cell.2021.04.048>.
73. Hafemeister C, Satija R. Normalization and variance stabilization of single-cell RNA-seq data using regularized negative binomial regression. *Genome Biol*. 2019;20:296. <https://doi.org/10.1186/s13059-019-1874-1>.
74. Wu T, Hu E, Xu S, Chen M, Guo P, Dai Z, et al. clusterProfiler 4.0: A universal enrichment tool for interpreting omics data. *Innovation (Camb)*. 2021;2:100141. <https://doi.org/10.1016/j.xinn.2021.100141>.
75. Street K, Risso D, Fletcher RB, Das D, Ngai J, Yosef N, et al. Slingshot: cell lineage and pseudotime inference for single-cell transcriptomics. *BMC Genomics*. 2018;19:477. <https://doi.org/10.1186/s12864-018-4772-0>.

Publisher's Note

Springer Nature remains neutral with regard to jurisdictional claims in published maps and institutional affiliations.

Ready to submit your research? Choose BMC and benefit from:

- fast, convenient online submission
- thorough peer review by experienced researchers in your field
- rapid publication on acceptance
- support for research data, including large and complex data types
- gold Open Access which fosters wider collaboration and increased citations
- maximum visibility for your research: over 100M website views per year

At BMC, research is always in progress.

Learn more biomedcentral.com/submissions

